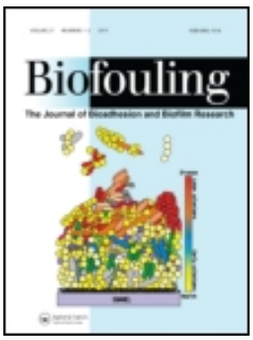

Biofouling

ISSN: 0892-7014 (Print) 1029-2454 (Online) Journal homepage: http://www.tandfonline.com/loi/gbif20

Corrosion of mild steel underneath aerobic biofilms containing sulfate-reducing bacteria part II: At high dissolved oxygen concentration

Whonchee Lee , Zbigniew Lewandowski , Mike Morrison , William G Characklis , Recep Avci & Per H Nielsen

To cite this article: Whonchee Lee , Zbigniew Lewandowski , Mike Morrison , William G Characklis , Recep Avci & Per H Nielsen (1993) Corrosion of mild steel underneath aerobic biofilms containing sulfate-reducing bacteria part II: At high dissolved oxygen concentration, Biofouling, 7:3, 217-239, DOI: 10.1080/08927019309386255

To link to this article: https://doi.org/10.1080/08927019309386255

Biofouling, 1993, Vol. 7, pp. 217–239
Reprints available directly from the publisher
Photocopy permitted by license only

CORROSION OF MILD STEEL UNDERNEATH AEROBIC BIOFILMS CONTAINING SULFATE-REDUCING BACTERIA PART II: AT HIGH DISSOLVED OXYGEN CONCENTRATION

WHONCHEE LEE*, ZBIGNIEW LEWANDOWSKI*, MIKE MORRISON*, WILLIAM G CHARACKLIS*, RECEP AVCI** and PER H NIELSEN***

*Center for Interfacial Microbial Process Engineering, Montana State University, Bozeman, MT 59717, USA; **Physics Department, Montana State University, Bozeman, MT 59717, USA: *** Environmental Engineering Laboratory, University of Aalborg, Denmark*

(Received 1 September 1992; in final form 20 March 1993)

Microbial biofilms containing sulfate-reducing bacteria (SRB) and general anaerobic bacteria (GAB) were grown in a closed flow channel reactor in air-saturated bulk liquid. The SRB proliferated within anaerobic microniches even when dissolved oxygen penetrated the entire biofilm at some locations. Corrosion of mild steel during aerobic/anaerobic biofilm accumulation was classified as aerobic corrosion and SRB-enhanced corrosion. Aerobic corrosion dominated during the early stages of biofilm accumulation. The corrosion rate decreased as the biofilm became more uniform over the surface. SRB-enhanced corrosion occurred after the SRB community was established within the deposits and significant amounts of iron sulfides contacted the bare steel surface. The initiation and propagation of SRB-enhanced corrosion in an aerobic/anaerobic biofilm system was explained through the establishment of an FeS/Fe galvanic cell.

KEYWORDS: biofilm, sulfate-reducing bacteria, corrosion, mild steel

INTRODUCTION

When local biofilm respiration rate is higher than DO transport rate, dissolved oxygen penetrates the biofilm only partially, which results in the formation of an anaerobic zone in the biofilm. In a companion paper (Lee *et al.*, 1993), results were presented on aerobic/anaerobic biofilm accumulation and corrosion of mild steel at a low bulk DO concentration (1.5 $mg \cdot l^{-1}$). SRB-enhanced corrosion under the aerobic/anaerobic biofilm was significantly higher than that under a totally anaerobic biofilm (Lee & Characklis, 1993). In a totally anaerobic biofilm, the nature and extent of corrosion was closely related to the ferrous sulfide accumulated within biofilm. In the aerobic/anaerobic biofilm, the aerobic process dominated corrosion during the early stages of biofilm accumulation. Iron hydroxides were the major corrosion products, which were more easily converted into sulfides and caused more serious corrosion than the bare steel. This led to the conclusion that the presence of iron oxides as well as the SRB activity are important in establishing the SRB-related corrosion.

Under abiotic, aerobic conditions, the corrosion rate of mild steel is proportional to bulk DO concentration (Uhing, 1971). Consequently, more iron hydroxides accumulate on the steel surface at high bulk DO concentration than at low bulk DO concentration.

In an aerobic/anaerobic biofilm system, SRB activity is enhanced in the anaerobic zone near the steel surface. Anaerobic conditions promote the transformation of iron oxides to iron sulfides. This results in SRB-enhanced corrosion. It is hypothesized that the higher the bulk DO concentration, the more pronounced is the SRB-enhanced corrosion. However, this mechanism has limitations. An increase in bulk DO concentration causes an increase in the depth of dissolved oxygen penetration into the biofilm which affects the proliferation of SRB.

The objectives of this work were: (1) to investigate the influence of the increased bulk DO concentration on SRB-related corrosion, and (2) to compare SRB proliferation within the biofilm at different bulk DO concentrations.

The experiment was conducted using air-saturated influent. Other parameters were the same as described in a companion paper (Lee *et al.*, 1993).

The formation of elemental sulfur and/or pyrite on a mild steel surface was accompanied by a high corrosion rate in an oxic/anoxic environment in the presence of SRB (McKenzie & Hamilton, 1992). To relate the presence of different sulfide compounds to corrosion rate, concentrations of elemental sulfur, acid-volatile sulfides (AVS) and chromium-reducible sulfide (CRS, mainly pyrite) within the deposits were measured periodically. A dissolved sulfide (DS) microelectrode was used to quantify the dissolved sulfide concentration within fouling deposits and near the metal surface. Scanning electron microscopy (SEM) and energy dispersive x-ray analysis (EDAX) were used to determine the spatial correlation of sulfide compounds with corroded pit occurrence.

MATERIALS AND METHODS

The experimental system, operating conditions, measurements, and analysis were described in a companion paper (Lee *et al.*, 1993). The modifications were as follows:

Flush Mounted Probes

In order to monitor biofilm accumulation in the channel reactor, a dissolved oxygen (DO) probe and transmission light sensors were flush-mounted in the channel reactor. The DO measurements were taken using a model 57 YSI meter and a model 5750 YSI DO probe (d = 1 cm) with a standard membrane. The transmission light measurements were performed using an infrared emitter/detector pair from Radio Shack (model 276–142). The DO concentration and light intensity were monitored using an interface and software from SCI Technologies, Incorporated. Data were collected and recorded every 10 min. The results of the optical measurements were expressed in terms of relative light intensity (I/I_o), where I_o was the intensity of the radiation incident (maximum radiation was determined at time zero); I was the emergent intensity. The information from flush-mounted probes was limited to the qualitative description of biofilm accumulation and DO penetration.

Chemical Analysis of Sulfide Compounds

Elemental sulfur, acid-volatile sulfides (AVS) and chromium reducible sulfide (CRS) were determined by modification of methods described by Fossing and Jorgensen (1989). The biofilm samples, removed from the reactor, were immediately fixed in 10 % zinc

acetate solution and preserved at 0° C. Elemental sulfur was extracted in ethanol and analyzed by high performance liquid chromatography (HPLC) using a UV detector. After extraction of elemental sulfur, AVS was determined by acidifying the sample with 6 N HCl and measuring the developed hydrogen sulfide. CRS was then determined using the balanced solution by cold reduction with chromium (II) in an acid solution under anaerobic conditions (Nielsen *et al.*, 1993).

Dissolved Sulfide Microelectrode

A 4 cm piece of platinum wire (d = 0.1 mm) was tapered by immersing it repeatedly in saturated KCN solution while applying 3 VAC between the wire and a graphite counter electrode. It required approximately 15 min to attain the desired taper. The tapered wire was inserted into a 5 cm length of 2 mm diameter lead glass tubing which had been previously heated and pulled down to a thin capillary. The tubing assembly was suspended from the top chuck of a pipet puller (Stoelting #51217). The heating coil was placed so that the top of the coil was 1.5 cm below the end of the tapered wire visible in the constricted tube. The end of the pulled pipet was ground flat on a rotating diamond impregnated wheel (Narishige Model EG–4). The platinum tipped pipet was recessed approximately 3 μm by immersing it in 0.1 M KCN and applying an anodic potential for 30 s. It was then rinsed with distilled water for 2 min. A layer of silver was plated on to the recessed platinum tip using Periodic Reverse Plating (PRP), (Hampel, 1964). In PRP, the surface was cycled between a reduction potential of –1.0 V for 1.0 s. and an oxidation potential of 1.0 V (*vs* Ag/AgCl reference) for 0.75 s. Cycling was repeated for 1 h to attain a smooth plating. The plating solution consisted of 0.53 g silver cyanide, 0.68 g potassium cyanide, 0.45 g of potassium bicarbonate, 0.1 g potassium hydroxide, all dissolved in 10 ml distilled water. The pH was 11.5–12. The electrode was then rinsed in distilled water for 2 min, immersed in 0.001 M sodium sulfide for 30 min, and again rinsed in distilled water. The resulting probe had tip diameter of approximately 50 μm. The method recommended by Hseu and Rechnitz (1968) was used to calibrate the microelectrode. A solution of known total sulfide concentration was prepared by diluting 1.0 M sodium sulfide stock solution to 0.01 M; the pH was 11.9. The sulfide probe and pH probe were then immersed in 100 ml of the solution. Electrode potentials were measured against a Ag/AgCl reference electrode. The pH was dropped by 1 pH unit at a time using hydrochloric acid down to pH 3. The pH and the sulfide potentials were recorded at each step. Based on pH (measured at each point) and total sulfide (known from the original sodium sulfide solution), the concentration of $S^{=}$ was calculated. The curve was linear down to pS 18 with a slope of 29.6 mV/pS. For the dissociation constants of hydrogen sulfide a pK_1 7.0 and 14.0 were used.

The dissolved sulfide microelectrodes were mounted on miromanipulators and penetrated the biofilm perpendicular to the metal surface. Dissolved sulfide concentration was measured in 100 μm intervals.

SEM/EDAX Analysis

Sample preparation for the cross sectional coupon with attached biofilm was described in the companion paper (Lee *et al.*, 1993). The sample was coated with an Au-Pd alloy and examined with a ISI-40 scanning electron microscope. Corrosion products were analyzed with the SEM and a Princeton Gamma-Tech System 4 Energy-dispersive X-ray Spectrometer (EDAX).

RESULTS

Substrate Removal and Biofilm Development

The experiment was conducted for 8 weeks. Organic carbon removal rate rapidly increased to about 2.5 g·[m^{-2}·d^{-1}] by the end of the fifth day, then slowly increased to about 3 g·[m^{-2}·d^{-1}] by the end of the second week, and then remained constant until the end of the eighth week (Fig.1). Oxygen removal rate was about 1.2 g·[m^{-2}·d^{-1}] by the end of the fifth d and increased to about 1.5 g·[m^{-2}·d^{-1}] by the end of the second week, then remained constant until the end of the eighth week (Fig.1). These results were consistent with those from the flush mounted DO and light sensors (Fig. 2). During the first week, the surface DO concentration decreased from 5.2 to 2 mg·l^{-1}, and the relative light intensity decreased from 1 to 0.65. From the second week to the fourth week, the surface DO concentration decreased to about 0.5 mg·l^{-1}, and the relative light intensity decreased to about 0.39, and then both remained constant until the end of the eighth week. The organic carbon in the effluent was between 2 and 3 mg·l^{-1}. Sulfate concentration was about 250 mg·l^{-1}. Sulfide was not detected in the bulk liquid during the entire experiment.

The average film thickness (biofilm + corrosion products) increased from approximately 1.2 mm by the end of the first week to about 3 mm by the end of the eighth week (Fig. 3). Surface area density of SRB increased from 1.5×10^7 cells·cm^{-2} by the end of the first week to 3.2×10^8 cells·cm^{-2} by the end of the sixth week (Fig. 4). Surface area density of heterotrophic bacteria and GAB increased slightly from the first week to the second week (from 1.2×10^9 to 3.2×10^9 cells·cm^{-2} for heterotrophic bacteria and from 1.7×10^8 to 2.8×10^8 cells·cm^{-2} for GAB) and then remained constant until the end of the eighth week. This was consistent with the organic carbon and dissolved oxygen removal rates which levelled off after approximately 10 days. The numbers of

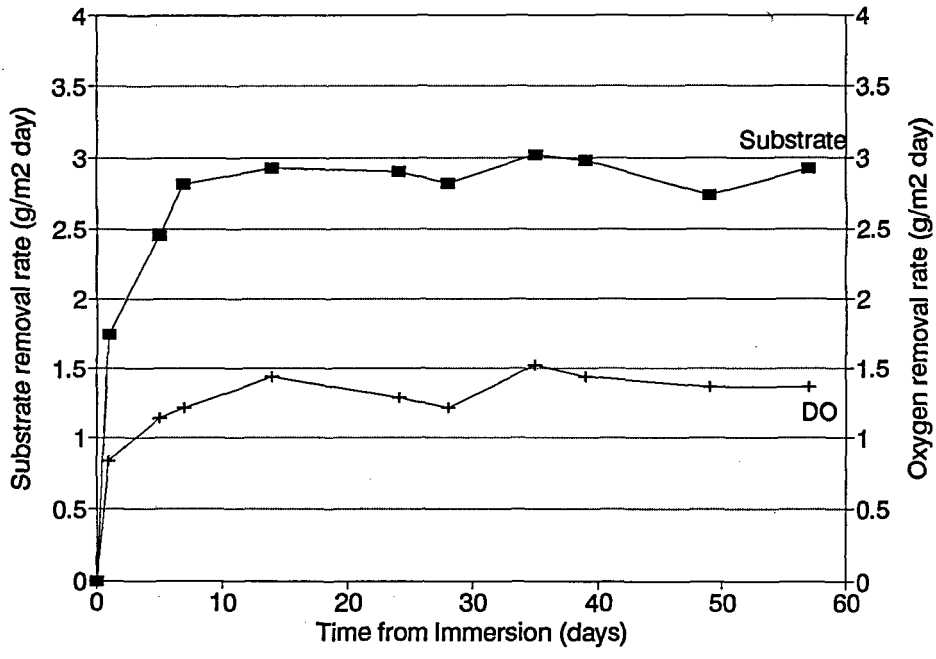

Fig. 1 Substrate (■) and oxygen removal (+) rates at different time periods.

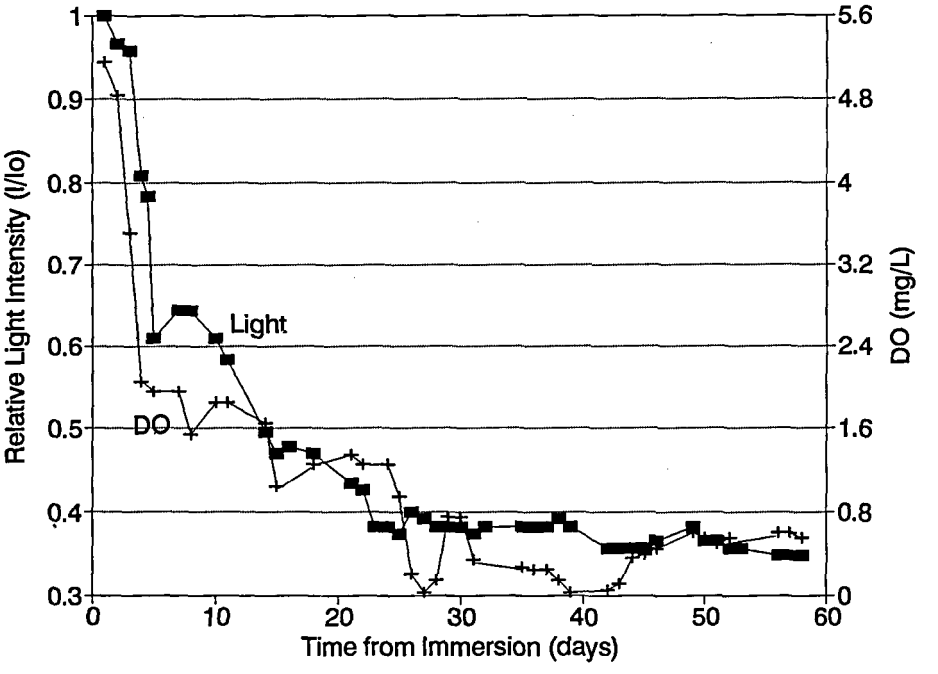

Fig. 2 Dissolved oxygen concentration (+) and relative light intensity (■) at flush mounted probes at different time periods.

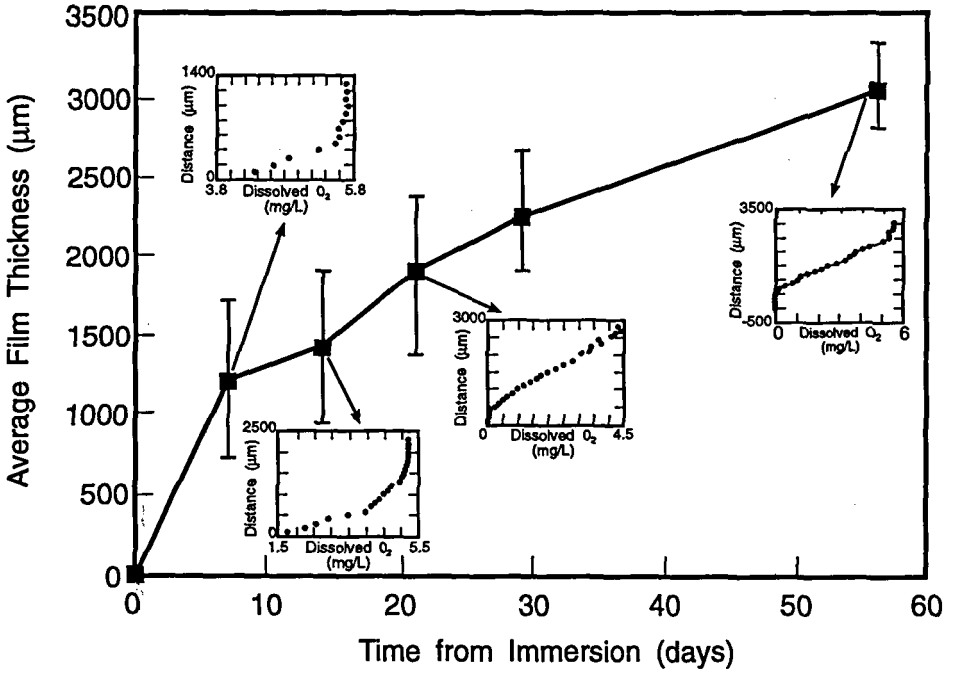

Fig. 3 Progression of fouling deposit thickness and corresponding DO profiles. Metal surface is indicated at distance = 0 only for the first two DO profiles.

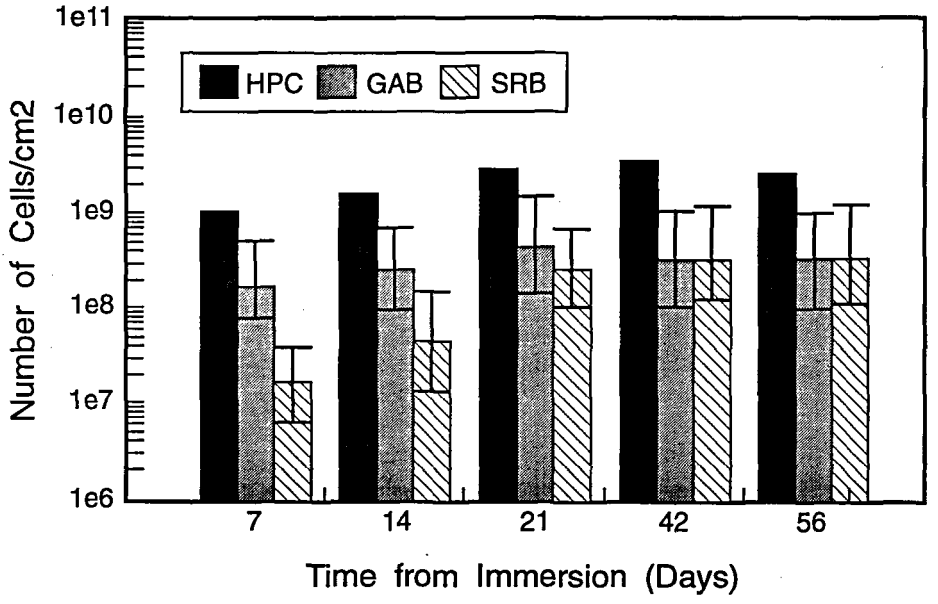

Fig. 4 Microbial accumulation in biofilm at different time periods. The bars indicate 95% confidence limits.

heterotrophic bacteria were between one and two orders of magnitude higher than those of SRB and GAB within the fouling deposits during the entire experiment (Fig. 4).

DO, DS, and pH Gradients Within the Deposits

Microelectrode measurement indicated that a DO concentration near the metal-deposit interface decreased from around 4 $mg \cdot l^{-1}$ by the end of the first week to approximately 1.5 $mg \cdot l^{-1}$ by the end of the second week, and to zero by the end of the third week (Fig. 3). These numbers reflect the trend only because the DO microelectrode measurements showed variation in DO distribution near the steel surface due to the biofilm heterogeneity. For example, two DO profiles indicated that DO concentrations near the steel surface were 0 and 1.8 $mg \cdot l^{-1}$ at different locations by the end of the fourth week (Fig. 5).

Measurements with DS microelectrode indicated SRB activity in the anaerobic zone near the steel surface at the end of experiment. The total dissolved sulfide concentration near the steel surface was about 10 $mg \cdot l^{-1}$ and decreased rapidly to 0 at a distance 300 μm from the steel surface (Fig. 6).

The pH, 6.9, was constant across the biofilm due to a considerable buffering capacity of the system (Fig. 6).

Corrosion Rate of Mild Steel During Biofilm Accumulation

Corrosion coupons covered with biofilm were periodically removed from the channel reactor, then fixed, embedded in polymer, and vertically sectioned. Microscopic observation of the cross sections revealed a layered structure of accumulated corrosion products underneath the biofilm throughout the entire duration of experiment. Corrosion products consisted of an outer orange material, an intermediate black zone, and inner deposits (Fig. 7). From the second week to the fourth week, pits were always observed under the orange deposit (Fig. 8). Tubercles, mainly composed of a dense layer of iron

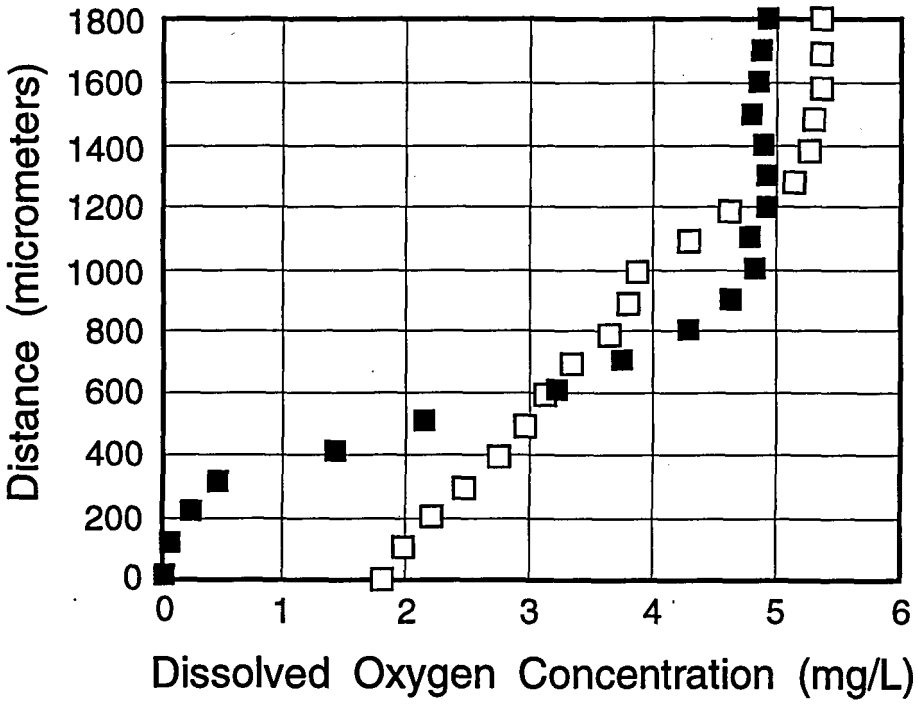

Fig. 5 Two DO profiles at different locations along the same metal coupon at the fourth week. Metal surface is indicated at distance = 0.

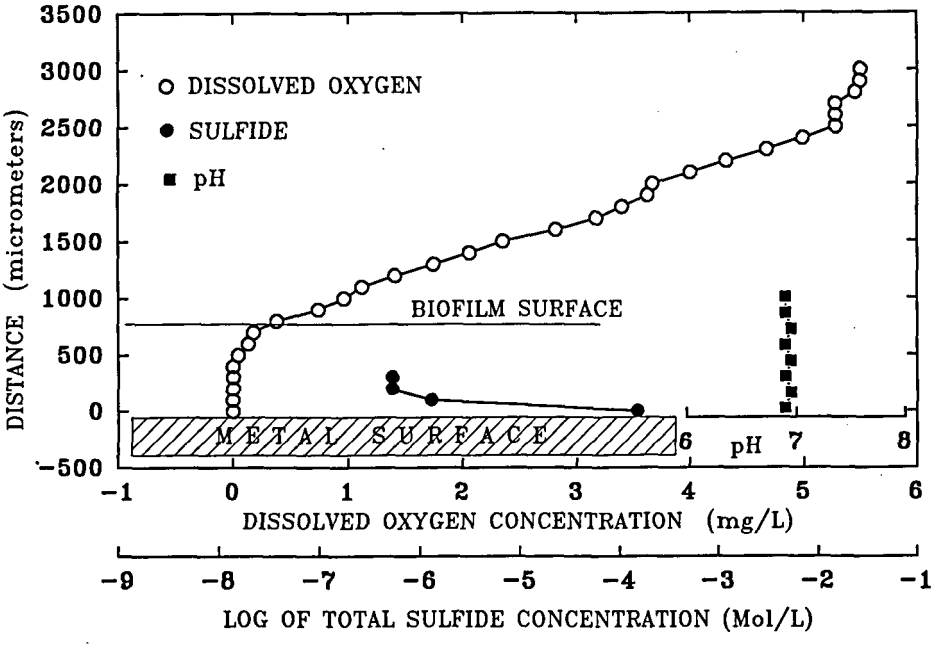

Fig. 6 pH, DO, and DS profiles through a biofilm to the metal surface at the end of the eighth week.

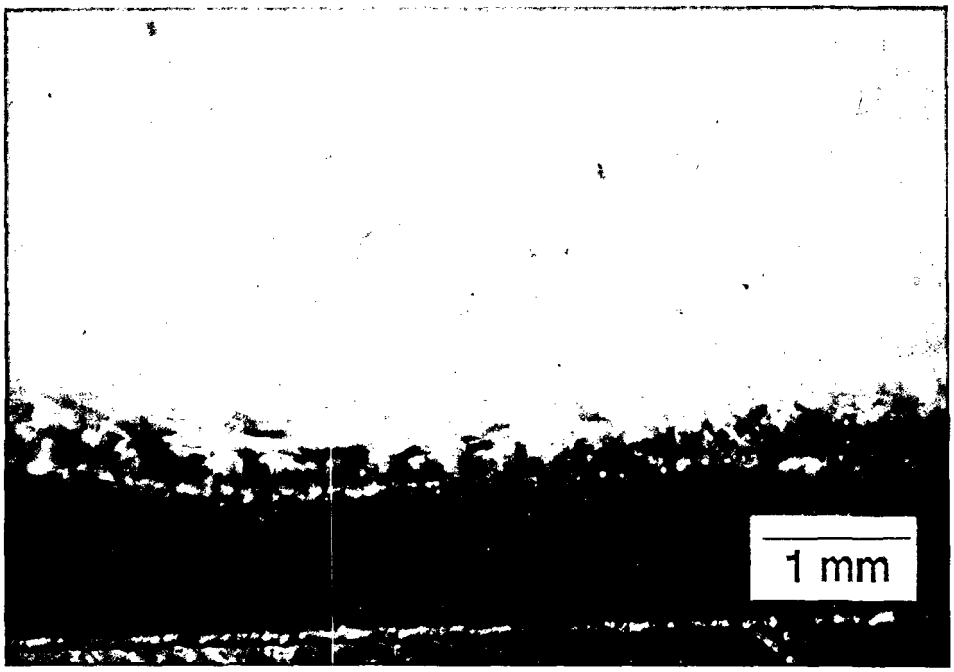

Fig. 7 Optical micrograph of a general corroded steel coupon and fouling deposits at the second week based on cross sectional observation. (See colour section)

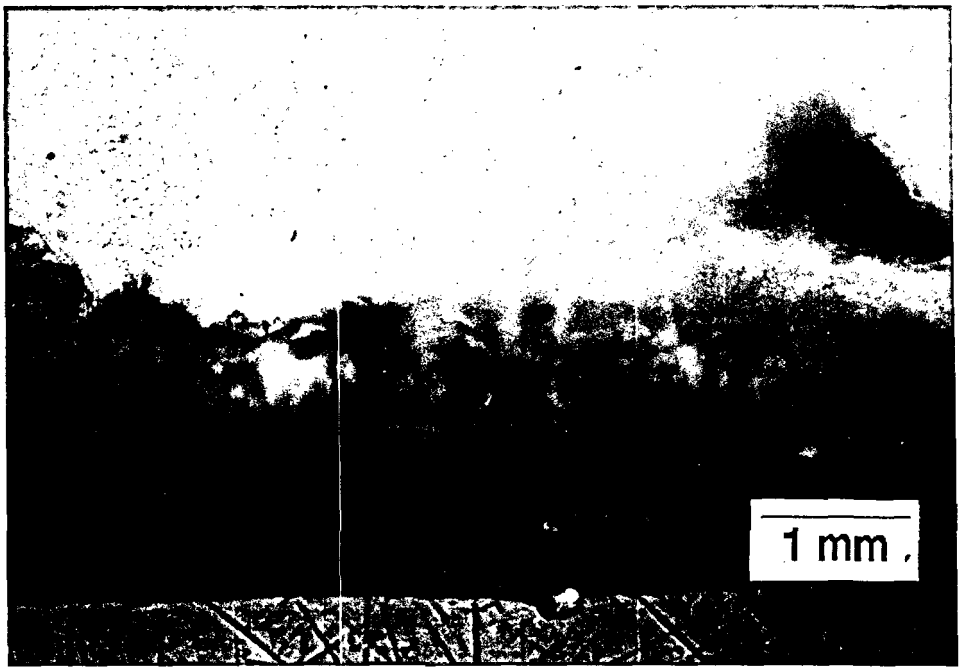

Fig. 8 Optical micrograph of a pitted steel coupon and fouling deposits at the second week based on cross sectional observation. (See colour section)

oxide, were found within fouling deposits at the end of the second week (Fig. 9). SEM/EDAX detected chlorine and phosphorus in the middle layer of the tubercle. Phosphorus was also detected at the bottom of the tubercle. No sulfur was detected around the tubercle areas at that time. From the sixth week to the eighth week, SRB-enhanced corrosion was visually observed after the film was removed (Fig. 10). The localized attack, shown in Figure 10 as a black area, eventually spread over the entire metal surface. A concentrated or eccentric ring structure with a pit at the bottom was always detected within the localized corrosion areas (Figs 11, 12). X-ray mapping of the cross section of a corroded coupon at the end of the eighth week indicated an iron sulfide film formed around the localized corrosion areas (Fig. 13).

DC polarization measurements showed no significant change in both anodic and cathodic current from the end of the first week to the end of the third week (Fig. 14a). The anodic and cathodic currents remained constant from the end of the fourth week to the end of the sixth week, but both increased by the end of the eighth week (Fig. 14b). The open circuit corrosion potential shifted in the negative direction (about 60 mV) from the first day to the end of experiment (Fig. 15). AC impedance plots indicated that only one time constant determined the corrosion reaction at open circuit corrosion potential (Figs 16 a, b). The polarization resistance (R_p) increased rapidly from 160 ohms by the second day to 1800 ohms by the end of the second week, and 2100 ohms by the end of

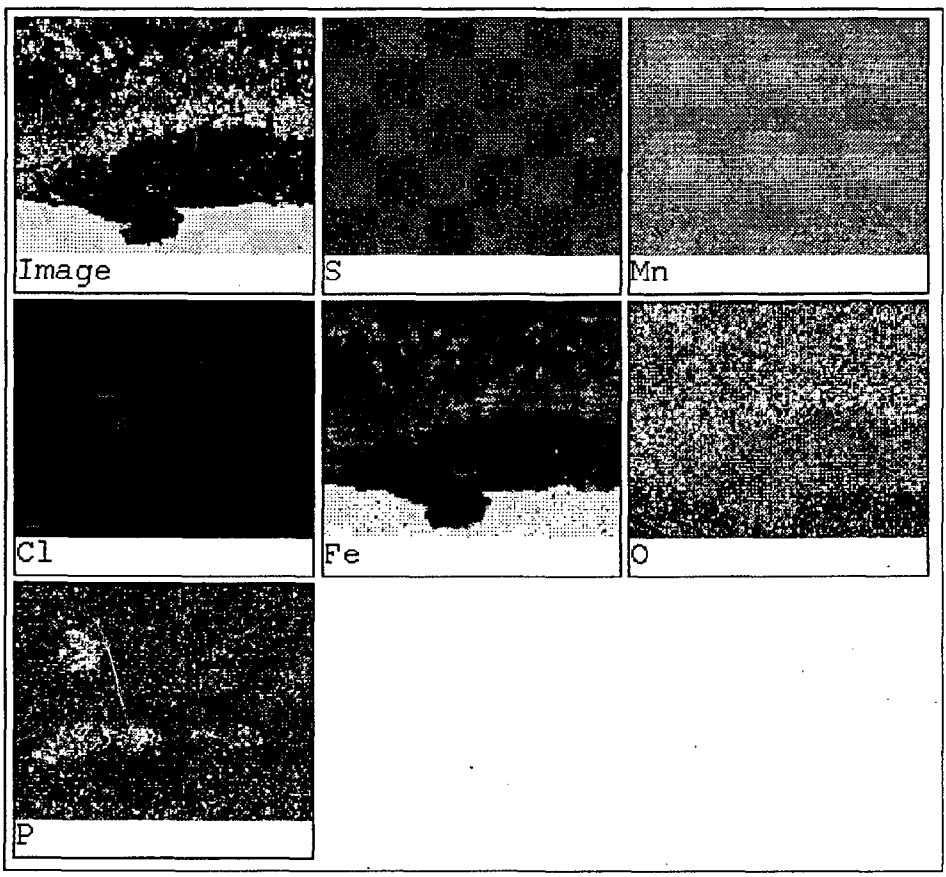

Fig. 9 X-ray map of Figure 8, showing the elemental distribution within a tubercle. (See colour section)

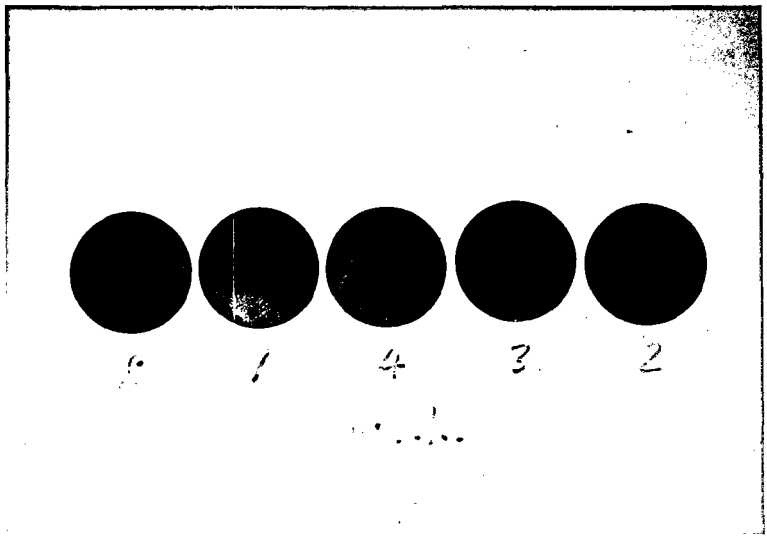

Fig. 10 Optical micrograph of corroded steel coupons after biofilm and corrosion products have been removed at different time periods. Black areas indicated the sulfide attack. (See colour section)

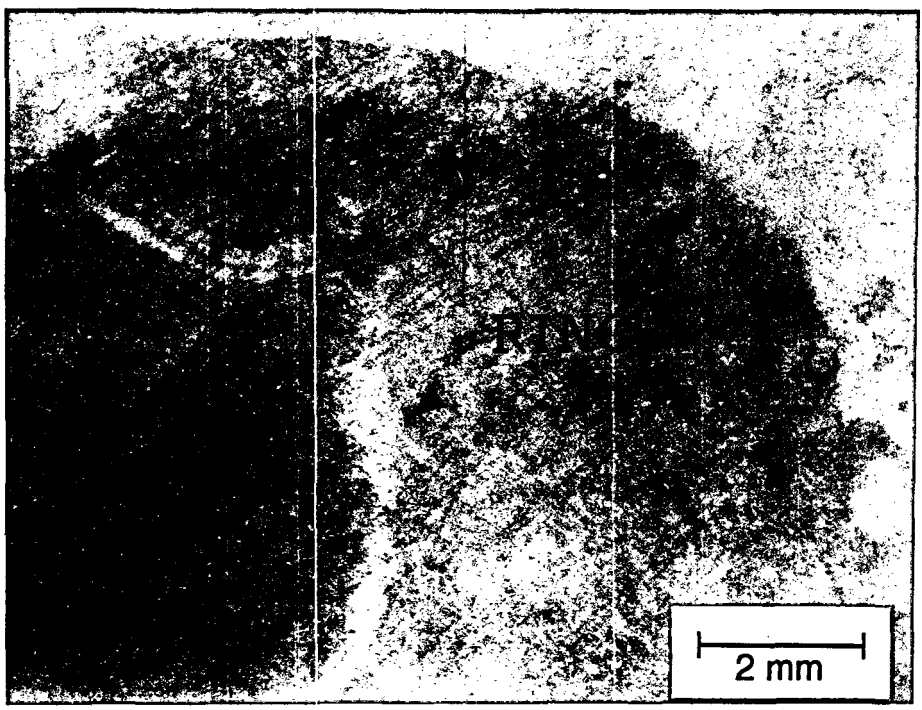

Fig. 11 SEM micrograph of a corroded steel coupon following removal of biofilm and corrosion products at the end of the eighth week. A ring structure (arrowheads) occurred in localized corrosion areas.

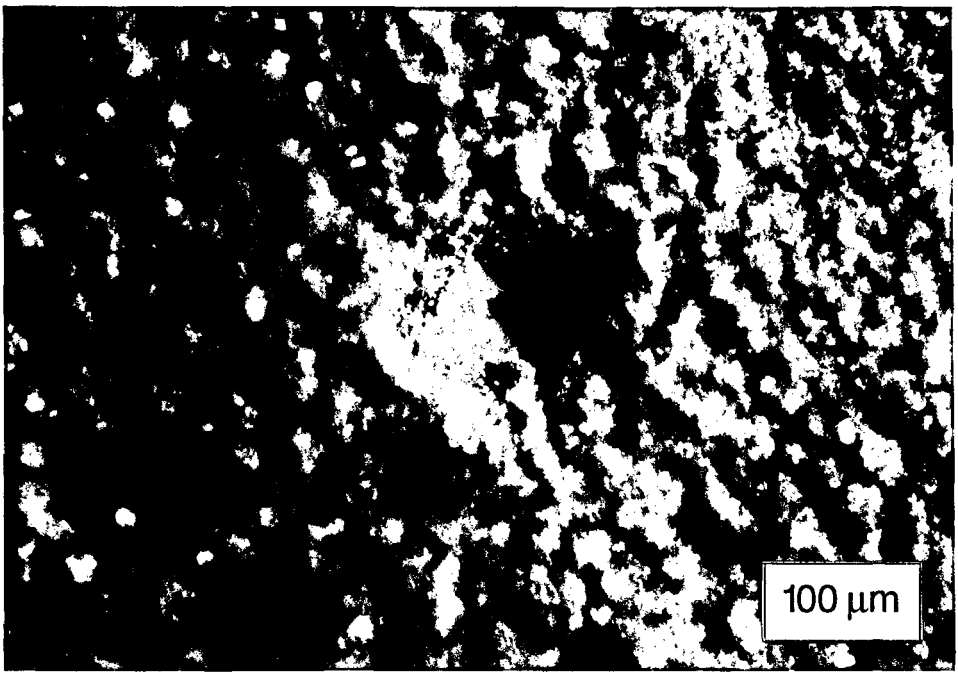

Fig. 12 Optical micrograph at the end of the sixth week of pitted steel in the sulfide-attacked areas caused by SRB. (See colour section)

the third week. The R_p decreased again to 1200 ohms by the end of the eighth week. The solution resistance (R_s) was constant, about 30 ohms during the entire experiment. AC impedance data indicated an initial decrease followed by an increase of corrosion rate with time. The error (R_s/R_p) in the DC measurements was estimated to be between 1.5% and 3.3% after the first week. Consequently, it can be assumed that the polarization curves were not distorted by the solution resistance.

The rates of corrosion calculated from polarization resistance during aerobic corrosion were higher at high bulk DO concentration than at low bulk DO concentration (Fig. 17).

Analysis of Sulfide Compounds Within Fouling Deposits

Acid-volatile sulfides within fouling deposits increased from 0.2 $\mu gS \cdot cm^{-2}$ by the end of the second week to 6.3 $\mu gS \cdot cm^{-2}$ by the end of the eighth week. Chromium reducible sulfide (pyrite) increased from 1.7 $\mu gS \cdot cm^{-2}$ by the end of the first week to 4.1 $\mu gS \cdot cm^{-2}$ by the end of the eight week (Fig. 18). Elemental sulfur, 1.6 $\mu gS \cdot cm^{-2}$ was detected only at the end of the eighth week.

AES Analysis

During the first 3 weeks, no sulfur was detected at the steel surface. Traces of sulfur and chlorine were detected on both pitted and non-pitted areas after the second week

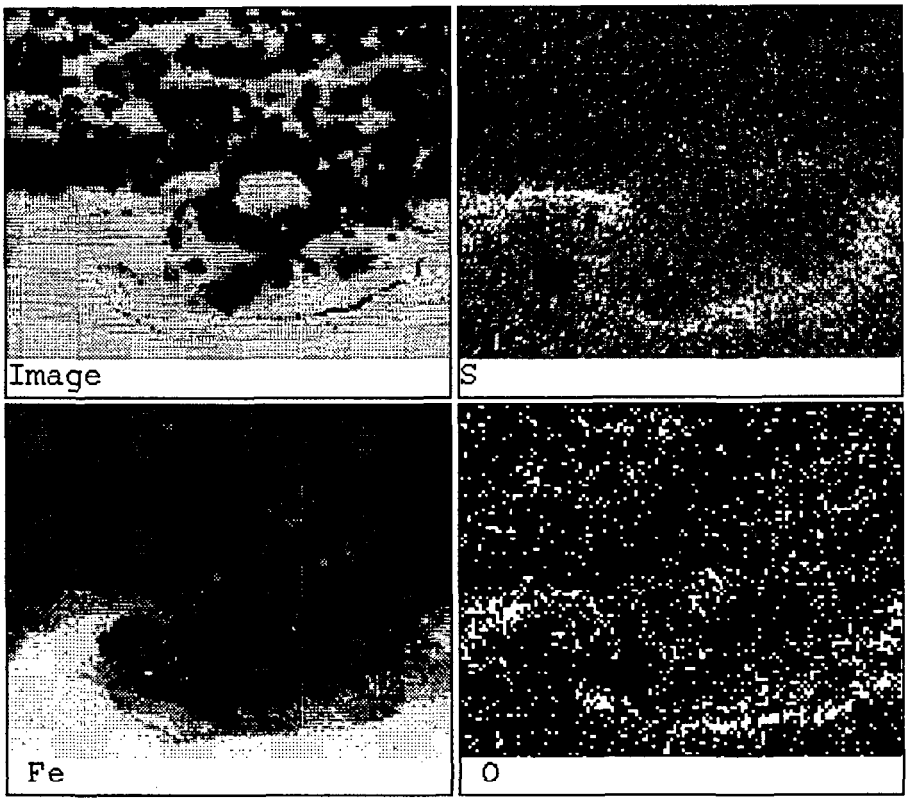

Fig. 13 X-ray map of a cross sectional coupon which showed a conductive iron sulfide film around the localized corrosion area at the end of the eighth week. (See colour section)

(Fig. 19). At the end of the sixth week, results from elemental mapping of the sulfide-attacked areas showed intermixed sulfur and oxygen (Figs 20 a, b, c). Sulfur was predominately located in the cracked and pitted areas observed in Figure 20 (a), whereas, oxygen was mostly distributed in the flat areas observed in Figure 20 (a). This observation was consistent in all the areas studied.

DISCUSSION

Oxygen Penetration and SRB Biofilm Development

The results indicated that SRB proliferated in a biofilm under air-saturated bulk liquid. Proliferation of SRB within the aerobic biofilm was limited by organic carbon, as demonstrated by the high sulfate concentration (about 250 $mg \cdot l^{-1}$) and low soluble organic carbon concentration (2 to 3 $mg \cdot l^{-1}$) in the effluent.

Oxygen removal rate followed the substrate removal rate. Microelectrode measurements indicated that dissolved oxygen penetration was different at different locations (Fig. 5). The depth of oxygen penetration was influenced by: (1) the local respiration rate of aerobic bacteria, (2) H_2S reacting with dissolved oxygen (and/or iron

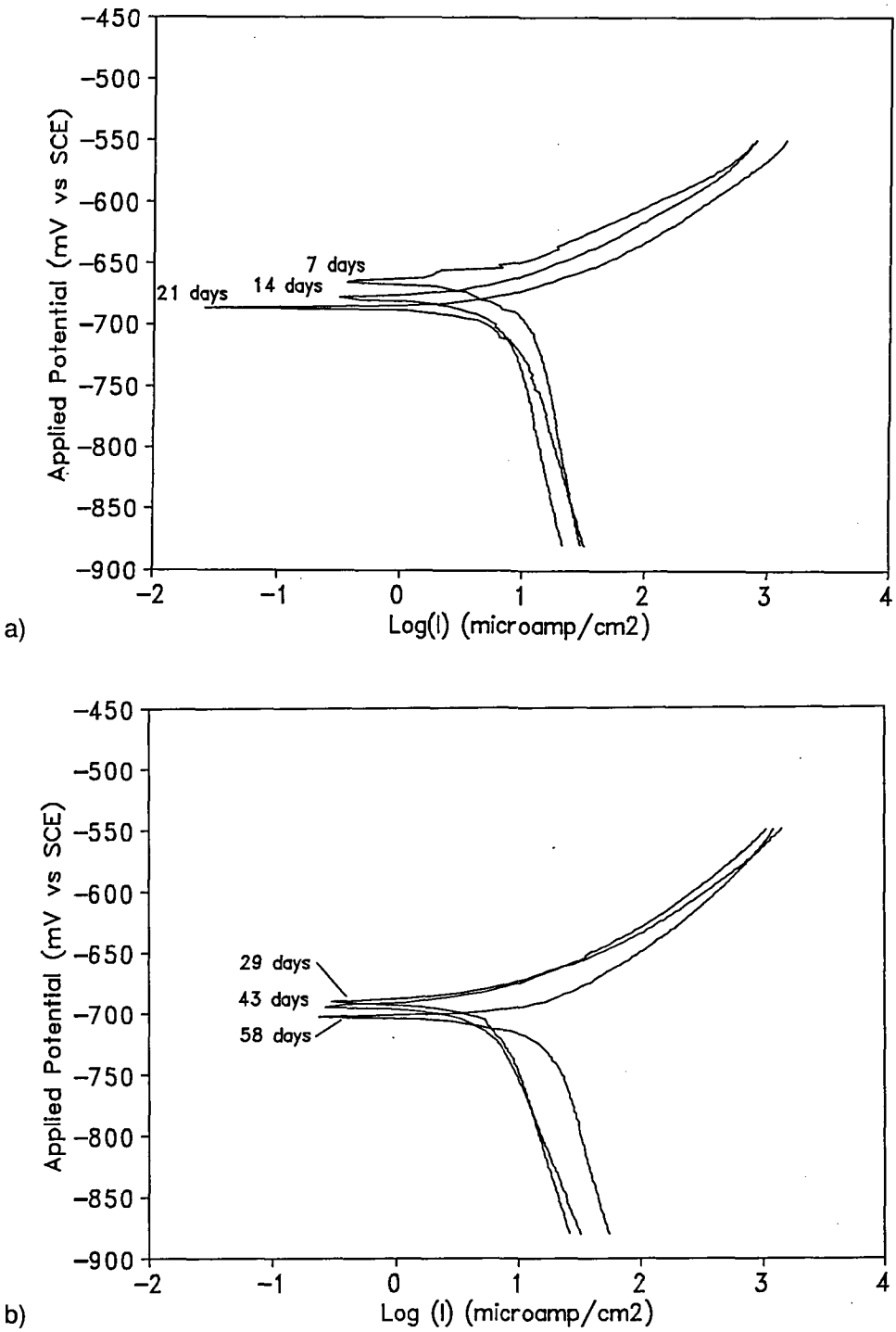

Fig. 14 (a) Anodic and cathodic polarization curves for the first three weeks; (b) anodic and cathodic polarization curves for the last three weeks.

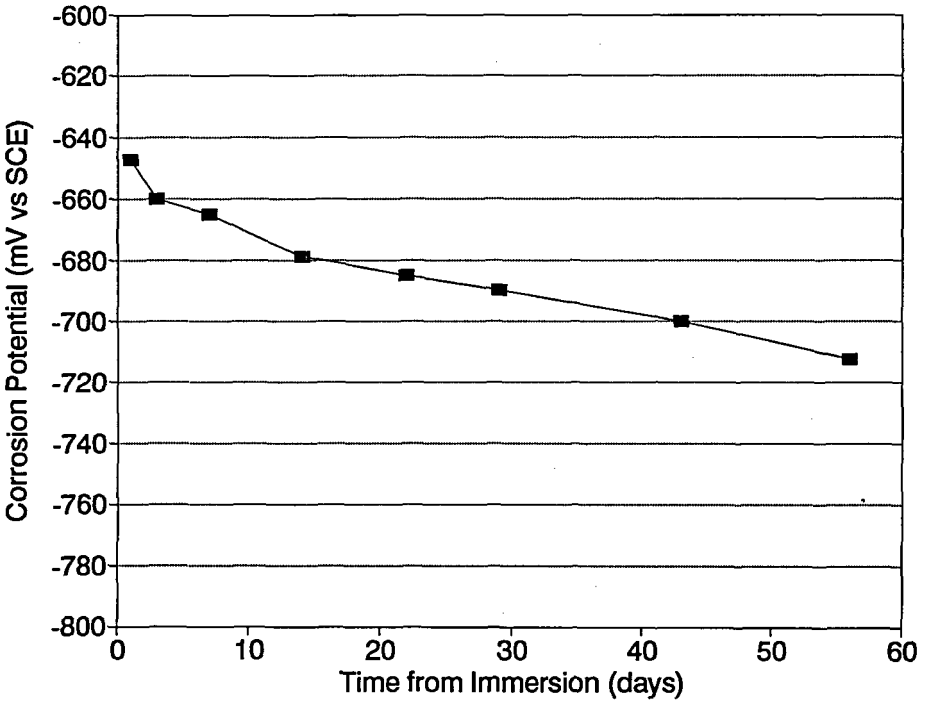

Fig. 15 Open circuit corrosion potential at different time periods.

oxide), (3) the local thickness of the deposit, which obstructs oxygen penetration, and (4) fluid dynamics.

At the end of the first week, the deposit thickness was about 1.2 mm. The increased deposit thickness may be beneficial for the growth of SRB at high DO concentration. Increased SRB numbers (Fig. 4) and increased concentration of sulfide compounds (Fig. 18) indicated that SRB proliferated after the first week. During the first 2 weeks, microelectrode measurements indicated that a DO concentration near the steel surface was between 4 and 1.5 $mg \cdot l^{-1}$. The mixed population biofilm was heterogeneous in terms of the spatial distribution of microbial species.

The results clearly demonstrate that SRB could proliferate in anaerobic microniches even when dissolved oxygen penetrated the entire biofilm at some locations.

Sulfide Reaction and Transport Within the Deposits

Sulfate reduction was occurring mainly near the steel surface where the conditions were anaerobic. An internal reoxidation of the produced sulfide within the biofilm by dissolved oxygen and ferric/ferrous hydrates may prevent sulfide build-up outside the biofilm. Absence of sulfide in the bulk liquid and an increase in sulfide compounds within fouling deposits indicate that H_2S precipitated as iron sulfides. Low corrosion rate and trace amounts of sulfur at the metal surface during the first month indicated that H_2S produced by SRB was reacting with either dissolved oxygen or the iron oxides precipitated around SRB colonies. The rate of abiotic sulfide oxidation by dissolved oxygen at pH 7 is very slow compared to that by iron oxides (Chen & Morris, 1972). Consequently, initial sulfide oxidation is dominated by the reaction

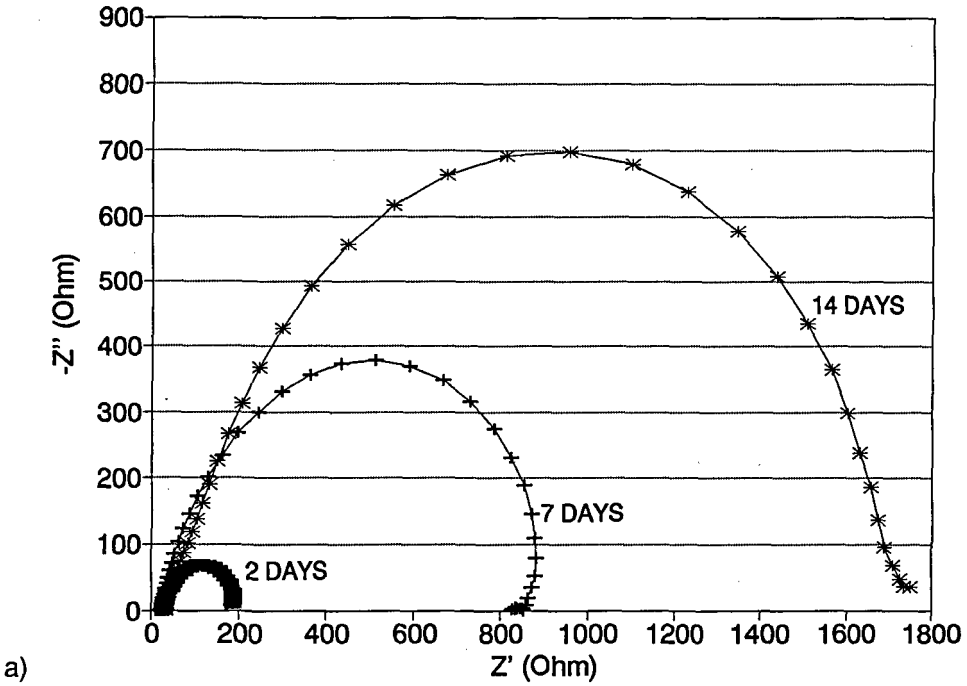

a)

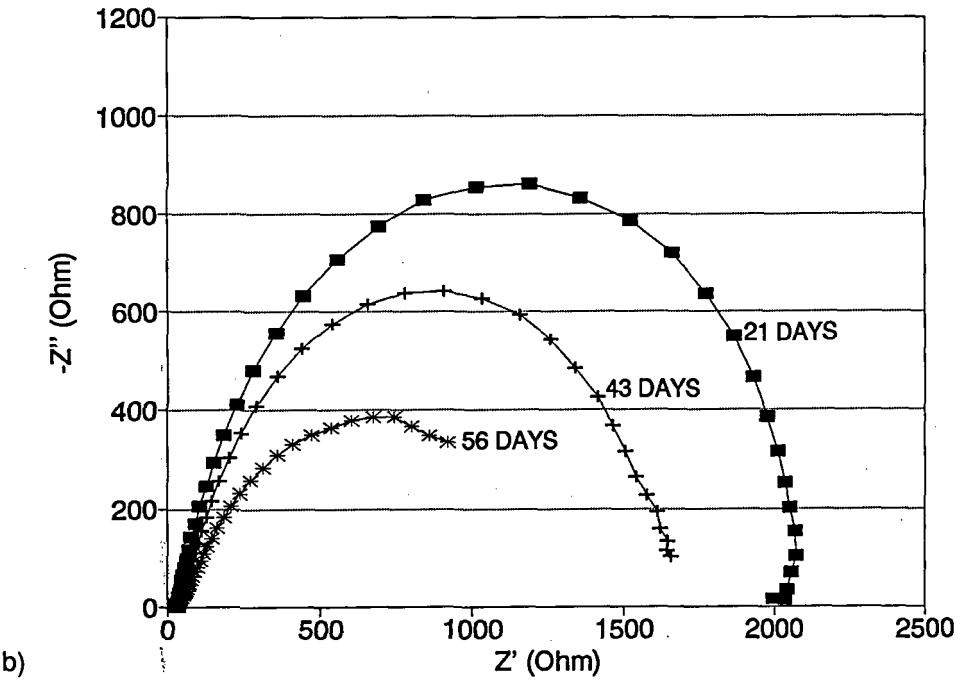

b)

Fig. 16 (a) Nyquist plots for the first two weeks; (b) nyquist plots for the last five weeks.

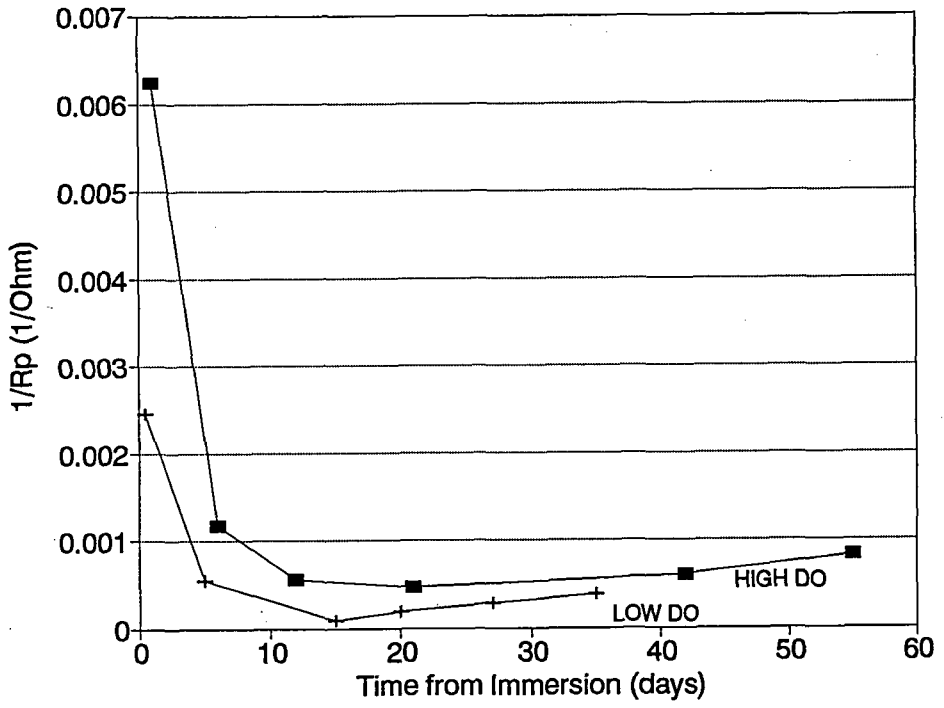

Fig. 17 Inversion of polarization resistance of mild steel at low (+) and high (■) bulk DO liquid at different time periods.

$$3H_2S + 2FeO(OH) \rightarrow 2FeS + S^\circ + 4H_2O \quad (1)$$

Chen and Morris indicated that polysulfide ions, S_x^{-2}, may be formed through the interaction of elemental sulfur and dissolved sulfide:

$$HS^- + (x-1)S \rightarrow H^+ + S_x^{-2} \quad (2)$$

in which S_x^{-2} is a polysulfide with x = 2 – 5. The polysulfide is highly reactive and can combine with ferrous ion and dissolved hydrogen sulfide to form pyrite at room temperature (Luther 1991):

$$Fe^{+2} + S_4S^{-2} + HS^- \rightarrow FeS_2 + S_3S^{-2} + H^+ \quad (3)$$

Equations (1)–(3) may explain the presence of pyrite within the deposits. SRB activity resulted also in accumulation of mackinawite or greigite in the deposits. Elemental sulfur and dissolved sulfide were also detected at the end of the experiment. The presence of dissolved sulfide, detected by the sulfide microelectrode, reconfirms the conclusion that the corrosion products near the metal surface at the end of experiment were iron sulfides.

It has been shown that mackinawite is the major corrosion product when iron alloys corrode in the presence of SRB, under totally anaerobic conditions (McNeil & Little, 1990). AVS (mackinawite or greigite) and CRS (pyrite) were detected in the

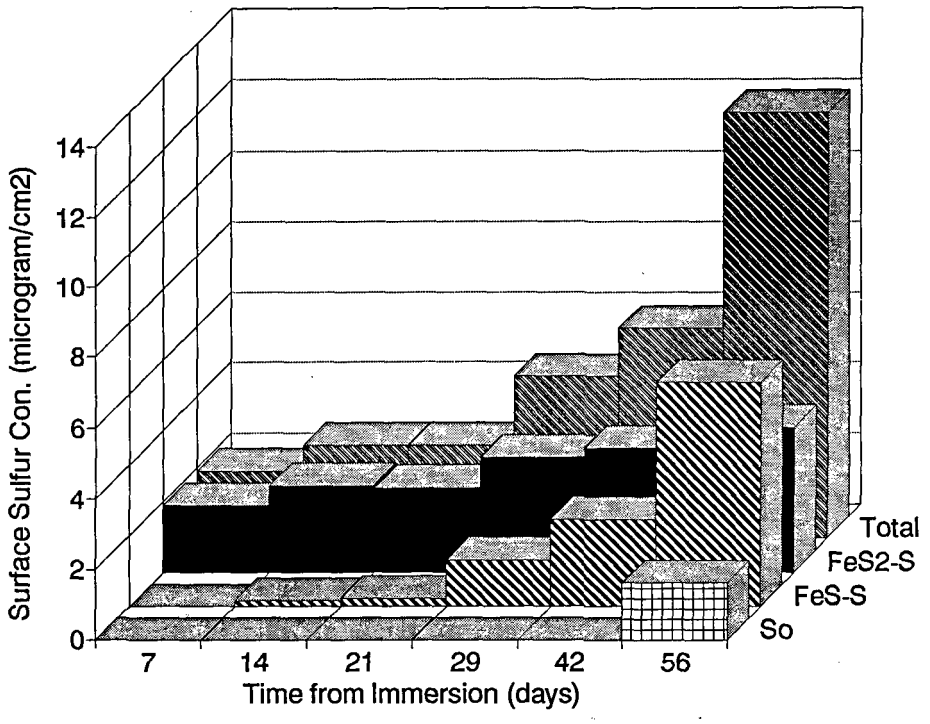

Fig. 18 Accumulation of acid-volatile sulfide (FeS) (▨), chromium reducible sulfide (FeS_2)(■), and elemental sulfur (S_o)(▦) at different time periods.

aerobic/anaerobic biofilm system. Both AVS and CRS concentration increased with time until the end of the eighth week.

Corrosion Process and Mechanism

The corrosion of mild steel during aerobic/anaerobic biofilm accumulation can be classified as aerobic and SRB-enhanced corrosion. Aerobic corrosion dominated during the early stages of biofilm accumulation. The corrosion rate decreased with time, and the access of dissolved oxygen to the steel surface became limited as biofilm became more continuous over the steel surface. SRB-enhanced corrosion occurred after establishment of the SRB population and after a significant amount of iron sulfide had contacted the steel surface. The increased corrosion rate caused by SRB activity at high DO concentration was accelerated by both the anodic and cathodic reactions (Fig. 14 b).

Comparison of Results with Those Obtained at Low Bulk DO Concentration

During aerobic corrosion, the rates of corrosion calculated from polarization resistance (Fig. 17) were greater at high bulk DO concentration than at low bulk DO concentration (Lee *et al.*, 1993). The deposit thickness increased from 1.2 mm by the end of the first week to 1.8 mm by the end of the third week at high bulk DO concentration and from

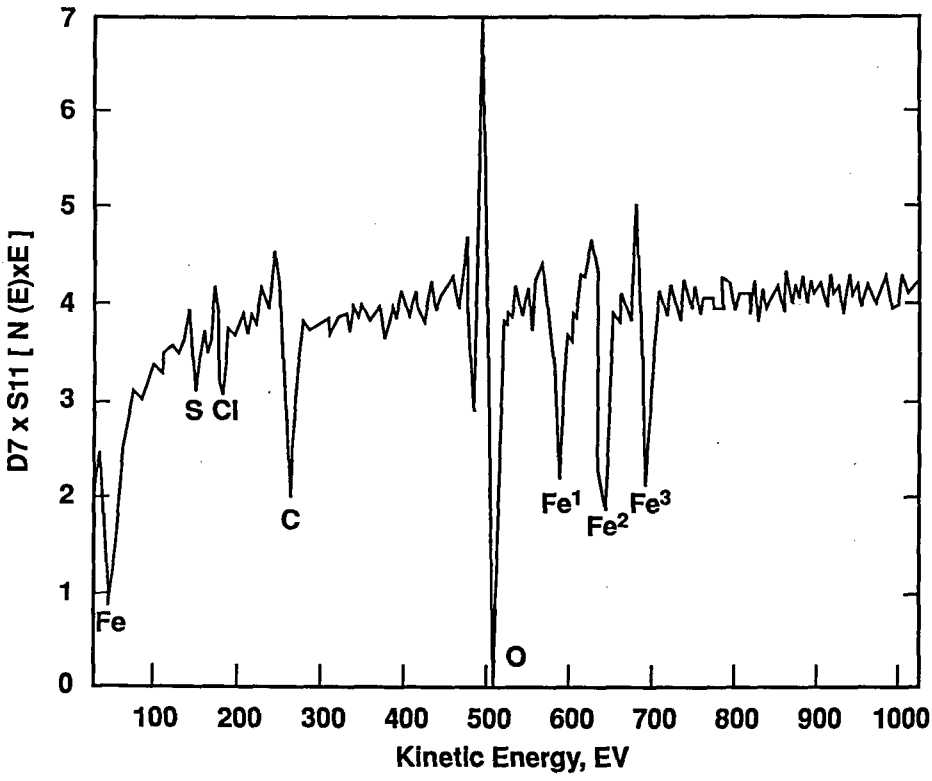

Fig. 19 Auger electron spectroscopy data for 1018 mild steel at the end of the second week.

0.4 mm to 1.2 mm at low bulk DO concentration. The thicker deposits at the higher bulk DO concentration may be attributed to the higher corrosion rate.

The structure of deposits and corrosion behavior were different at high and low bulk DO concentration. At high DO bulk concentration, layered corrosion products were observed under the biofilm throughout the entire experimental periods (8 weeks). The layered structure consisted of an outer orange deposit, an intermediate black zone, and the inner corrosion products. Pits were always located directly under the orange deposit during aerobic corrosion (Fig. 8). There was no evidence of sulfur accumulation, suggesting that the localized accelerated pitting was caused by the infusion of dissolved oxygen. SRB-enhanced corrosion was initiated with localized attacks after 6 weeks, which eventually spread over the entire steel surface (Fig. 10). Deep pits were observed within localized corrosion areas caused by sulfide attack.

At low bulk DO concentration, the deposit layers were different from those at high bulk DO concentration. A top layer of brownish ferric hydrate was formed initially, and this turned black after 4 weeks. A uniform adherent black iron oxide film was observed during aerobic corrosion. SRB-enhanced corrosion also initiated localized attack after 3 weeks. No deep pitting was observed at that time.

It appears that abiotic, oxidative processes occur faster than biotic respiration processes during the early stage of biofilm accumulation. This results in more pits and higher corrosion rate at high bulk DO concentration than at low bulk DO concentration.

The accumulation of biofilm, corrosion products, and the history of corroded steel during aerobic corrosion may affect the SRB-related corrosion. At low bulk DO concentration, several sulfide-attacked areas were observed. Small, shallow pits (about 10 μm in diameter) were concentrated within the larger corroded area. At high bulk DO concentration, initial sulfide attack seemed to concentrate in one spot. Large, deep pits (about 100 μm in diameter) were observed within the sulfide attacked areas (Fig. 12). The SRB-enhanced corrosion at high bulk DO concentration was further characterized by a periodic eccentric or concentric ring structure with well-defined edges between adjacent rings (Fig. 21).

Initiation and Propagation of SRB-enhanced Corrosion

In a totally anaerobic system, the importance of iron sulfide to the corrosion of mild steel in the presence of SRB has been emphasized. King *et al.* (1973) indicated that the corrosion of mild steel in the presence of SRB is principally due to their ability to produce ferrous sulfide in a semi-continuous culture experiment. Lee and Characklis (1993) proved that corrosion of mild steel is accelerated only when the iron sulfide particles physically contact the steel surface in a biofilm reactor. In the described experiment, after SRB activity developed, the corrosion rate remained stable for some time, and then increased rapidly. This induction period for SRB-enhanced corrosion in an aerobic environment may correspond to the time necessary for the iron sulfide to accumulate and make direct contact with the steel surface. During aerobic corrosion the steel surface is initially covered with amorphous corrosion products, bacterial cells, and extracellular polymeric materials (Little *et al.*, 1990). These deposit materials can react with H_2S and/or act as a diffusion barrier for H_2S or iron sulfides in reaching the metal surface. The heterogeneous nature of biofilm accumulation may result in localized iron sulfide accumulation, which explains the initial localized attack. The attacked surface areas increased in size as sulfide deposits increased. This reinforces the galvanic cell theory of SRB-enhanced corrosion. (King & Wakerley, 1973). The DS microelectrode measurement, surface analysis (SEM/EDAX and AES), and polarization measurements also support this theory. At the end of the experiment, the DS concentration was highest at the steel surface where iron sulfide had precipitated. The x-ray mapping of the cross sectional corroded coupon showed the enrichment of sulfur at the bottom of the localized corrosion area. The cathodic and anodic current increased somewhat at that time.

The initiation of SRB-enhanced corrosion in an aerobic/anaerobic biofilm can be explained by establishment of a galvanic cell, FeS/Fe, whereby the iron becomes anodic. The cathodic reaction, hydrogen evolution, occurs on the biogenic iron sulfide. The propagation of SRB-enhanced corrosion is attributed to the increased SRB activity and the increased contact area of iron sulfides with the bare steel. The ring structure of corrosion pattern may reflect the history of SRB-enhanced corrosion. Deep pits are caused by a large ratio of cathode/anode area (Fig. 22).

CONCLUSION

The bulk liquid concentration of dissolved oxygen affects SRB-related corrosion. The corrosion rate under totally anaerobic conditions was negligible compared to that under aerobic conditions (Lee & Characklis, 1993). Maximum corrosion rate and deepest pitting during aerobic corrosion were observed when the bulk liquid was saturated with air. The dissolved oxygen influences SRB-related corrosion either indirectly through the

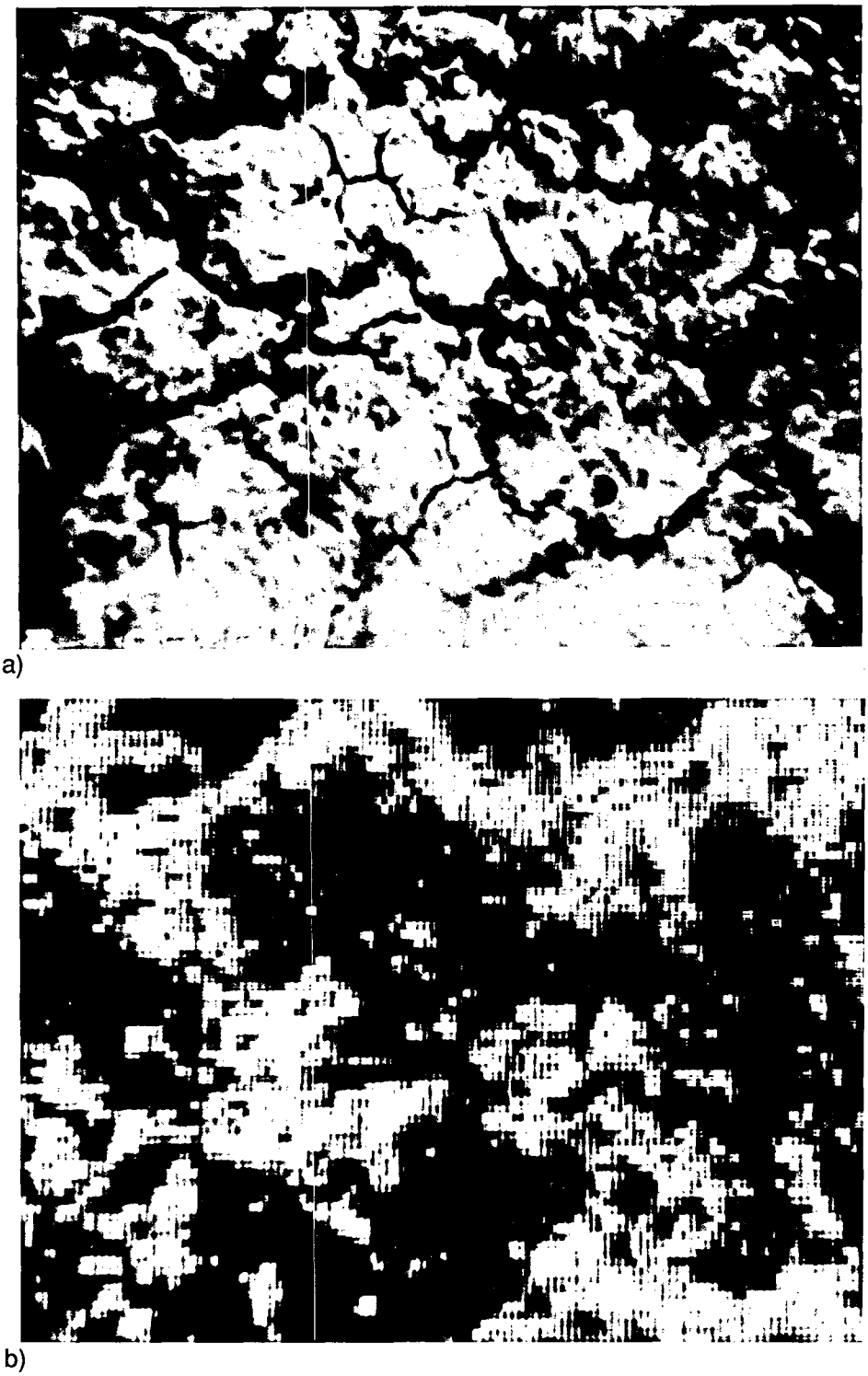

Fig. 20 (a) Auger electron micrograph of mild steel after argon ion sputtering for 30 min at the end of the sixth week; (b) sulfur Auger electron map of Fig. 19; (c) oxygen Auger electron map of Fig. 19.

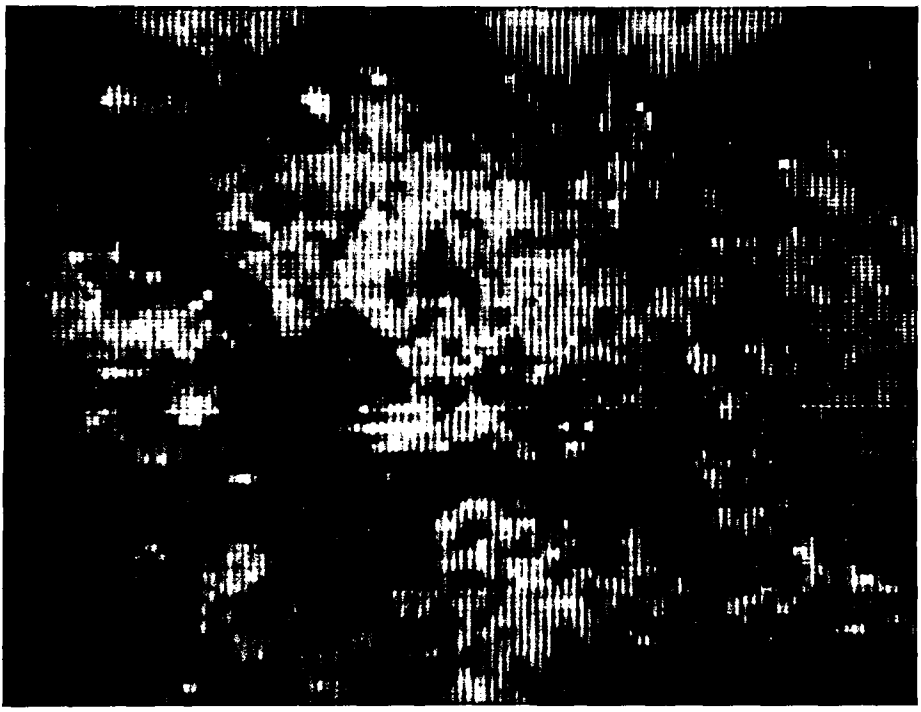

c)

Fig. 20 (c)

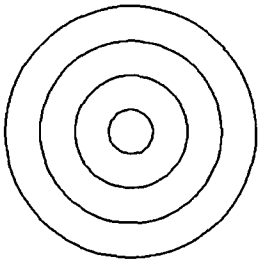

Fig. 21 Characteristic ring structure of corroded steel caused by SRB in high bulk DO liquid.

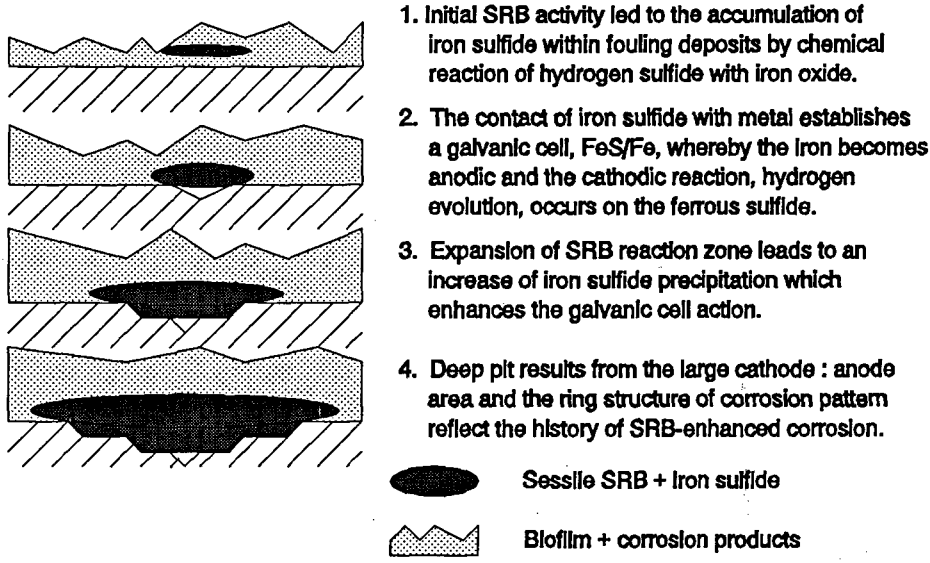

Fig. 22 Sequence of SRB-enhanced corrosion of mild steel in high bulk DO liquid.

formation of corrosion products (ferrous or ferric hydroxides, elemental sulfur, and pyrite) or directly, acting as a cathodic depolarizer. The direct effect of dissolved oxygen on the cathodic reaction is unlikely under the reported experimental conditions. The surface DO concentration decreased to zero and the surface DS concentration was about 10 $mg \cdot l^{-1}$ at the end of the eighth week. The pyrite and elemental sulfur present in fouling deposits are known to be more corrosive toward steel than mackinawite (King *et al.*, 1973). It is not clear to what degree each of these compounds contributes to corrosion.

Based on the results described, the following can be concluded: 1. Mixed population biofilms are heterogeneous with respect to the spatial distribution of microbial species. SRB can proliferate in anaerobic microniches even when dissolved oxygen penetrates the entire biofilm at some locations. 2. The presence of dissolved oxygen significantly increases the amounts of pyrite and elemental sulfur, in addition to mackinawite or greigite, in the deposits. 3. SRB-enhanced corrosion begins as localized attack which is eventually propagated over the entire steel surface. This corrosion is significant only when there is a conductive iron sulfide deposit to establish a galvanic cell. 4. The influence of bulk DO concentration on SRB-related corrosion is significant. At low bulk DO concentration, several sulfide attacked areas were observed. Small, shallow pits were concentrated within the large corroded area. At high bulk DO concentration, initial sulfide attack was concentrated at one spot. Large, deep pits were observed within the sulfide attacked areas.

Acknowledgements

The authors express their appreciation to Dr V Griffths, Department of Metallurgy, Montana Tech. for making SEM/EDAX instrumentation available. DR F Mansfeld and R Xiaog, Department of Material Science, University of Southern California assisted in interpretation of AC impedance data. The authors also express their appreciation to

Ms Gail Callis for her assistance in metallographic support. Authors gratefully acknowledge the cooperative agreement ECD – 8907039 between Montana State University and National Science Foundation. The Center for Interfacial Microbial Process Engineering Industrial Associates are also acknowledged for their support of this work.

References

Chen K Y, Morris J C (1972) Kinetics of oxidation of aqueous sulfide by O_2. *Environ Sci Technol* **6:** 529–537

Fossing H, Jorgensen B (1989) Measurement of bacterial sulfate reduction in sediments: evaluation of a single step chromium reduction method. *Biogeochemistry* **8:** 205–222

Hampel C A (1964) *Encyclopedia of Electrochemistry.* Reinholdt Publishing Company New York, NY, pp 892–898

Hseu T, Rechnitz G A (1968) Analytical studies of a sulfide ion-selective electrode in alkaline solution. *Anal Chem* **40:** 1054–1060

King R A, Wakerley D S (1973) Corrosion of mild steel by ferrous sulfide. *Br Corros J* **8:** 41–45

King R A, Miller J D A, Smith J S (1973) Corrosion of mild steel by iron sulfides. *Br Corros J* **8:** 137–141

King R A, Miller J D A, Wakerley D S (1973) Corrosion of mild steel in cultures of sulfate-reducing bacteria: effect of changing the soluble iron concentration during growth. *Br Corros J* **8:** 89–93

Lee W, Characklis W G (1993) Corrosion of mild steel under an anaerobic biofilm. *Corrosion*, (in press)

Lee W, Lewandowski Z, Okabe S, Characklis W G, Avci R (1993) Corrosion of mild steel underneath aerobic biofilms containing sulfate-reducing bacteria part I: at low dissolved oxygen concentration. *Biofouling* **7:** 197–216

Little B J, Wagner P A, Characklis W G, Lee W (1990) Microbial corrosion. In: Characklis W G, Marshall K C *Biofilms.* John Wiley & Sons, New York, NY pp 635–670

Luther III G W (1991) Pyrite synthesis via polysulfide compounds. *Geochim cosmochim Acta* **55:** 2839–2849

McKenzie J, Hamilton W A (1992) The assay of *in situ* activities of sulfate-reducing bacteria in a laboratory marine corrosion model. Submitted to *Int Biodeterior Bull*

McNeil M B, Little B J (1990) Mackinawite formation during microbial corrosion. *Corrosion* **46:** 599–600

Nielsen P H, Lee W, Lewandowski Z, Morison M, Characklis W G (1993) Corrosion of mild steel in an alternating oxic and anoxic biofilm system. Accepted for publication in *Biofouling*

Uhing H H (1971) *Corrosion and Corrosion Control.* John Wiley & Sons, New York, NY, pp 93–96